THE ASTROPHYSICAL JOURNAL, 381:147–159, 1991 November 1

GLOBULAR CLUSTER MASS FUNCTIONS[1]

HARVEY B. RICHER AND GREGORY G. FAHLMAN
Department of Geophysics and Astronomy, University of British Columbia, Vancouver, BC, Canada V6T 1W5

ROBERTO BUONANNO
Osservatorio Astronomico di Roma, Viale del Parco Mellini 84, I-00136, Roma, Italy

FLAVIO FUSI PECCI
Dipartimento di Astronomia, Università di Bologna, via Zamboni 33, I-40126, Bologna, Italy

AND

LEONARD SEARLE AND IAN B. THOMPSON
The Observatories of the Carnegie Institution of Washington, 813 Santa Barbara Street, Pasadena, CA 91101
Received 1991 February 22; accepted 1991 May 6

ABSTRACT

Deep imaging data in the *I* bandpass for three globular clusters were used to construct their luminosity and mass functions. These new data for ω Cen, M5, and NGC 6752, together with existing data for M13, NGC 6397, and M71 were then employed to investigate any symptomatics of the cluster mass function slopes and their evolution. A related question also considered was the relation between the currently observed and the IMF slopes. While definitive answers regarding the evolution of globular cluster mass function slopes are not yet possible, mainly due to the small existing sample of observed mass functions extending down to low masses ($M < 0.2\ M_\odot$) and to restrictions in the theoretical modeling, certain trends are becoming apparent. In particular, it does appear that cluster evolution of stars has been important in modifying the cluster mass function slopes for at least two and possibly three of the clusters studied. A very important and quite robust result is that some (and perhaps all) clusters probably have very steep IMFs with the slope likely exceeding 2.5 (Salpeter value 1.3). This result suggests that low mass Population II stars may be an important component of the mass budget of the halo if the spheroid's mass function is similar to that seen in globular clusters.

Subject headings: clusters: globular — luminosity function — stars: low-mass

1. INTRODUCTION

Convincing evidence has been developed over the past few years that there is a major portion of the mass of the Galaxy that is emitting little or no radiation, or that it is putting out this energy in a frequency band that is as yet unexplored. A leading candidate for this dark matter, if it is baryonic, is low-metallicity brown dwarfs; stars with masses less than about 0.1 $M_\odot$ which are incapable of burning their nuclear fuel.

There are several reasons, however, why these objects have not as yet been widely accepted as the most probable dark matter candidates. First, searches for these stars have not been particularly successful (Jameson, Sherrington, & Giles 1983; Boeshaar, Tyson, & Seitzer 1986; Skrutskie, Forrest, & Shure 1987; Campbell, Walker, & Yang 1988). However, it may be that most of the searches thus far have been looking in the wrong places. If the dark matter is in brown dwarfs, then these stars will likely have a Galactic distribution similar to that of Population II objects, whereas the existing searches have generally been in Population I environs. The reason why these brown dwarfs are likely to have a halo distribution is that from the flat rotation curve of the Galaxy, the dark matter can be modeled most simply with a spherical halo of radius at least 35 kpc (Fich & Tremaine 1990). Stars in this halo would have formed in the earliest stages of formation of the Galaxy. Coupled with this is the possibility that low-mass stars are likely to be the favored mode of star formation in the metal-poor environments expected in the early stages of galactic evolution (Zinnecker 1987). Another problem has been a misconception concerning the actual number of discovered low-mass objects compared with the numbers expected from a halo dominated by brown dwarfs. For example, in the Boeshaar et al. (1986) survey, about a factor of 4 more faint subdwarf candidates were detected than expected, suggesting that current estimates of the low-mass stellar density in the halo (e.g., Chiu 1980; Dawson 1986) may be underestimates. The deep pencil beam survey of Cowie et al. (1988) produced faint star counts that are consistent with a very steep halo mass function. This is so because the Bahcall-Soneira (1981) Galaxy model that they used to interpret their counts (their counts were consistent with the predictions of this model) uses a constant luminosity function from the Wielen peak (see Wielen, Jahreiss, & Kruger 1983) down to $M_V = 16.5$. Because the mass-luminosity relation is falling so steeply in this region (VandenBerg & Bell 1985; D'Antona 1987), this extrapolation actually converts into an extremely steep mass function.

Earlier efforts by both Schmidt (1975) and Chiu (1980) yielded halo mass functions that were as steep as the Population I function (Chiu) or possibly significantly steeper (Schmidt). By contrast, Hartwick, Cowley, & Mould (1984) suggest that low-mass stars in the halo are not an important contributor to the Galactic dark matter unless the mass function turns up for very low masses.

A detailed search for very low mass halo dwarfs will be extremely time consuming and very large-telescope intensive. However, a search in globular clusters may be equivalent, and it will certainly be more efficient. If current pictures of the formation of the Galactic halo are correct (Larson 1976; Searle

[1] Based on data collected with the NTT at the European Southern Observatory and the du Pont Telescope, Las Campanas Observatory.

& Zinn 1978), then the present population of globular clusters is but a small fraction of those that were present initially (see, for example, Aguilar, Hut, & Ostriker 1988, hereafter AHO). The vast majority were destroyed through dynamical interactions in the early phases of evolution of the Galaxy, and their stars currently constitute some fraction of the Galactic halo. Whether the global halo mass function is similar to that of globular clusters is still not known, but if we take the simplest assumption that they are similar, knowledge of the low-mass stellar content in globular clusters may then be an important parameter in the halo mass budget. A major complication here will be accounting for the dynamical effects that have modified the presently observed globular cluster mass function slopes.

2. GLOBULAR CLUSTER MASS FUNCTIONS: THEN AND NOW

What we eventually seek in determining globular cluster mass functions are the cluster initial mass functions (IMFs) as it is the IMF which holds the clue to star formation scenarios and the importance of the low-mass stars. At the outset, this appears to be a difficult task as dynamical processes, both internal to the cluster and externally caused by the cluster's interaction with the Galaxy, have likely altered most clusters' currently observed mass functions. However, as was pointed out in Richer & Fahlman (1991), both Fokker-Planck and multimass King models of clusters demonstrate that if observations are obtained for very low-mass stars at large distances from the cluster core, the observed mass function slope is very similar to the IMF in the absence of extensive tidal stripping. This arises because the stars at large core distances are not in thermal equilibrium as are the stars near the cluster center because the relaxation time in the outer parts of most clusters exceeds the Hubble time. Even in the presence of a significant amount of tidal stripping, the observed mass function slope for the low-mass stars at large distances from the core still represents a lower limit to the IMF slope as low mass stars are preferentially removed in the stripping process.

This result is illustrated in Figure 1 where we present theoretical mass functions at differing core radii derived from a multimass King model. The input model contained 17 mass bins and had a power-law mass function with slope $x = 2.0$ which is a rough mean value of what we are seeing at the low-mass end in typical Galactic globular clusters (see § 4). For comparison, the Salpeter slope is 1.35. The particular model illustrated has a low-mass cutoff at 0.05 $M_{\odot}$ and, because of the steep mass function slope, about 53% of the total mass of the cluster is contained in stars with masses less than 0.12 $M_{\odot}$. The concentration parameter ($c = \log r_{\rm tidal}/r_{\rm core}$) for this King model is 1.4 for the giants ($M = 0.78\ M_{\odot}$) which is also typical of the clusters which we will discuss shortly. The mass functions at five selected radii are illustrated with the logarithm of the distance in units of the core radius (for the giants) shown to the left of each mass function. The input mass function (which is the IMF for this cluster as no tidal stripping can be included in King models) is indicated with the dotted line.

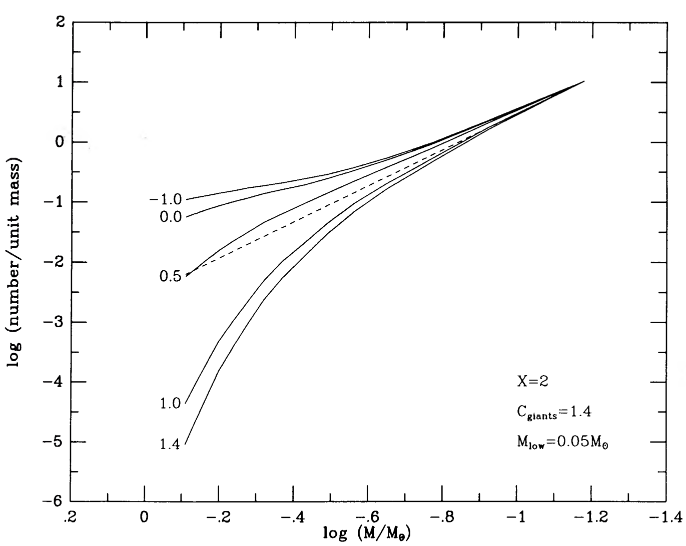

FIG. 1.—Mass functions at five different radii in a multimass King model. The cluster IMF is shown as the dotted line. Mass segregation is clearly seen in the most massive stars, but the lowest mass objects have a mass function slope that is similar to the IMF.

The effects of mass segregation on the most massive cluster stars can be seen clearly in Figure 1. The central regions of the cluster have an excess of the heaviest objects compared to a deficiency at the outer reaches of the cluster. What is important for our purposes is that the mass function slopes for the low-mass stars, particularly at large core radii, are similar to the cluster IMF. The measured mass function slopes at 3 and 10 core radii (0.5 and 1.0 in the log) are 1.8 and 2.2, respectively, for the lowest mass stars, nicely bracketing the IMF slope. What this means in practice is that we can recover real cluster IMFs by measuring their mass function slopes for low-mass stars at large core radii from the cluster centers. This statement is, of course, only true if (*a*) King models are reasonable approximations to real clusters and (*b*) the clusters have not undergone extensive tidal stripping. Point (*a*) is probably well satisfied for the majority of clusters as it is by now well known that luminosity profiles generated from King models fit most cluster profiles quite adequately (Djorgovski & King 1986). Further, as was shown in Richer & Fahlman (1991), results similar to Figure 1 can be obtained for Fokker-Planck calculations as well as King models, so that the effect is quite robust. Point (*b*) is more difficult. There is no doubt that at least some clusters have experienced extensive tidal stripping (e.g., E3 [McClure et al. 1985] and Pal 5 [Smith et al. 1986]), but the ones that are likely to have been most affected are those with small perigalactic distances and those whose orbits are only slightly inclined to the Galactic disk. For the clusters currently well removed from the Galactic center and at high Z distances, the expectation is that the extent of tidal stripping may be minimal. This borne out in the analysis of AHO who demonstrate that at the Sun's Galactic radius the most important mechanism for removal of stars from globular clusters is evaporation. In general, for these clusters this effect is about an order of magnitude more efficient than either bulge or disk shocking or dynamical friction. Since evaporation proceeds on a time scale that is generally long compared to a Hubble time for most clusters (AHO), we can anticipate that the IMFs of many clusters have not been extensively modified over the past Hubble time. This will be especially true for mass function slopes measured at about the cluster half-mass radius where we are far enough out in the cluster that the measured slope is near that of the IMF (see Fig. 1), but that we are not so far out that stripping has become important. Even in the cases where some or extensive modification has occurred, the currently observed global mass function slopes will be *flatter* than the IMF as stripping of stars from clusters preferentially favors the removal of low-mass stars which are less strongly bound than massive stars in a system in energy equipartition.

The conclusion that can be drawn from Figure 1 and the discussion above is that observed mass function slopes in real clusters obtained at moderately large radial distances for low-mass stars should be a reasonable approximation to the cluster IMF if the cluster has not been extensively tidally stripped. Even in the case of removal of stars by tidal interaction of the cluster with the Galactic disk and bulge, the observed cluster mass function slope will still represent a lower limit to the true IMF slope.

3. THE NEW DATA: ACQUISITION AND REDUCTION

In a recent paper (Richer et al. 1990), we reported on the results of a deep imaging survey in three globular clusters. What was learned in this study was that the mass functions in all these clusters turned up sharply at the low-mass end (below about 0.4 $M_\odot$), and that a mass function slope as steep as $x = 2.7$ was seen in M13 for the lowest mass stars. Within the framework of the discussion in § 2, this suggests that the IMF for this cluster at the low-mass end was at least this steep. The other two clusters examined (M71, NGC 6397) had much flatter mass function slopes, but both are dynamically much older than M13. This naturally led to the suggestion that we were observing in these systems a modification of their IMFs by dynamical processes. This is an important result bearing on the star formation mechanisms in the early universe (what determines the IMF in a globular cluster?), the destruction time scales of globulars (can the halo be composed of tidally destroyed clusters?), and the source of dark matter in the Galactic halo (if such steep mass function slopes continue down into the brown dwarf regime, and if the halo mass function is similar to that seen in these clusters, then low-mass stars could be a leading candidate for the Galactic dark matter). With only three deep mass functions available, however, any conclusions are tentative at best; an extension of the sample size is clearly required.

In 1990 May we used the NTT at ESO to survey three more clusters, two of which are expected to be dynamically young as their half-mass relaxation times exceed 2 Gyr (ω Cen $T_{1/2} = 9.1$ Gyr and M5 $T_{1/2} = 2.7$ Gyr, where $T_{1/2}$ is the cluster half-mass relaxation time taken from Webbink [1985] and Binney & Tremaine [1987]), while the final cluster, NGC 6752, has a half-mass relaxation time of 0.9 Gyr. In an earlier observing run (1989 May) with the du Pont Telescope at Las Campanas Observatory, some data in ω Cen were also obtained and are used in the analysis.

In all cases, the data consists of deep CCD I frames and less deep V exposures in both cluster and blank fields together with flat fields (done on the sky), bias frames, and exposures of standard stars (Landolt 1983; Schild 1984; and Searle & Thompson 1990). The blank fields were located outside each cluster's tidal radius (typically at about 1° away) at the same Galactic latitude as the cluster and were used to account for the field star and galaxy contamination to the star counts. All star counts discussed in the following sections are based on the I frames only. At ESO the CCD used was a 1024 × 1024 Thompson chip with 19 μm pixels. This pixel size projects to 0".15 on the sky. At Las Campanas, the CCD was a Texas Instruments chip with 15 μm pixels projecting to 0".16 on the sky. No fringing, even in I, was present in the data from either source. All CCD frames were preprocessed with routines in IRAF and the reductions were carried out using the version of DAOPHOT found in the same software package. The photometry on some of the frames was checked with the standard ROMAFOT code (Buonanno 1988) with practically indistinguishable results. Below we summarize the quantity and quality of data obtained for each globular cluster.

3.1. *ω Centauri*

The data for ω Cen consist of frames obtained from both observatories. The field observed at Las Campanas was selected from the finding chart produced by Alciano & Liller (1984, 1987) and is centered on their star "U." This field is located at about 19′ west of the cluster center. Eight frames, each with an exposure time of 450 s, were obtained in the cluster as well as in the blank field. A final averaged frame was produced in each instance, and it was this averaged frame that was eventually analyzed. The FWHM of the point-spread function on each of these final frames was 0".8. The photometry for both the cluster and blank fields was calibrated with standard stars in SA 110, SA 112, SA 113, and stars near PG 1323−085, all of which were measured by Searle & Thompson (1990). The ESO field was located 343″ east and 84″ north of the Las Campanas field at R.A. (1990) $13^h24^m51^s$ and decl. (1990) −47°22′07″, effectively at 13'.4 from the center. This field was selected to avoid bright stars on the frame. Because it is closer to the center, the stellar density is somewhat higher than in the Las Campanas field. In this case the data consist of nine 1200 s exposures in the cluster and seven 1200 s frames in the blank field. In both final averaged frames, the FWHM of a stellar image was about 0".9. All the ESO data were calibrated with standard stars in SA 110 and M67 (Schild 1984).

3.2. *M5*

The M5 data were not obtained under optimal seeing conditions with the final FWHM of the point spread function at 1".1. Five 1200 s frames were used in the cluster field, but only two were secured for the background. The seeing on these latter frames was somewhat better (1".0), and this coupled with the reduced crowding resulted in their going as deep as the cluster frames so that they were able to provide the required background corrections. The cluster field was centered at R.A. (1950) $15^h17^m39^s$, decl. (1950) +02°06′47″, and, at 400″ west of the cluster center, is located at about 14 core radii.

3.3. *NGC 6752*

The best data set that we secured was for NGC 6752. The final I frame consists of five 1200 s exposures, while the blank field contained six such exposures. In both data sets the final FWHM was 0".75. The cluster field for NGC 6752 was located at about 4′ east of the cluster center at R.A. (1990) $19^h10^m42^s$ and decl. (1990) −60°02′00″, just south west of stars 123 and 127 of Cannon & Stobie (1973). This corresponds to a distance from the cluster center of 8 core radii (the core radius assumed here is 30″ as given in Webbink 1985 even though the cluster is suspected of having a power-law luminosity profile in its inner regions [Djorgovski & King 1986]).

Note that in all the three globular clusters, the fields were located in the range of 6–14 core radii from their respective centers. By comparison with Figure 1, this implies that mass function slopes determined from the low-mass stars in these cluster frames ought to be representative of the IMF cluster slopes if extensive tidal stripping has not occurred in the clusters under study. This may be quite a reasonable assertion as the fields are all well inside the respective cluster tidal radii and hence the mass functions derived are for stars still strongly bound to their clusters.

4. REDUCTIONS AND DERIVED LUMINOSITY FUNCTIONS

Reduction of the frames was carried out on a Sun Microsystems 4/110 workstation with 32 Mbyte of core memory, using the Unix version of DAOPHOT embedded in IRAF. Even with such a relatively powerful workstation devoted exclusively to this project, the reductions still consumed several months of cpu time. The reductions were carried out along standard lines with two passes made through the data, the second pass meant to locate faint stars in the wings of brighter ones. Numerous ADDSTAR trials were carried out with the statistics of recovery of the added stars providing the incompleteness corrections to the counts. Figures 2 and 3 illustrate some of these results for NGC 6752. For the cluster field, a total of 3250 artificial stars were added in 13 separate trials (the frame being rereduced each time with the newly added stars included), while in the background frame 1250 stars were added in nine trials. These numbers ensured that the incompleteness corrections were accurate to better than 15% over the magnitude range of interest. In the data for the cluster field it is clear that the photometry remains reliable to about $I = 23.5$, with some bias toward recovering faint stars too bright at the dim end. This is easily understood as ease in recovery of faint stars if they happen to lie on positive noise peaks in the sky or on other faint stars. The background data are clearly reliable to fainter than $I = 24$ with very little evidence of any bias to this depth.

Luminosity functions for the fields in each cluster were calculated from star counts in cluster frames (corrected for incompleteness) minus the counts in the background frames (also corrected for incompleteness). These functions are discussed below for each cluster individually.

4.1. *Luminosity Function for ω Centauri*

The derived luminosity functions for the two fields in ω Cen are shown in Figure 4, the upper curve (greater star density) coming from the field at 13′.4 (ESO) and the lower one from Las Campanas data at 19′. The offset between the two curves, amounting to about 0.5 in the log, is consistent with the surface brightness profile for this cluster at these two radii (Meylan 1987). The details of the star counts are shown in Table 1, where the apparent I magnitude indicates the bin center with the counts done within ± 0.25 mag of the center, n are the incompleteness corrected counts with the subscript c referring to the cluster and b the background. In are the incompleteness corrections that were applied to the raw counts in order to derive the counts n, and Φ is the final luminosity function. The errors in Φ include those due to counting statistics in both the cluster and background fields as well as the errors associated with the incompleteness corrections. The observed counts may not be integral even when the incompleteness correction is

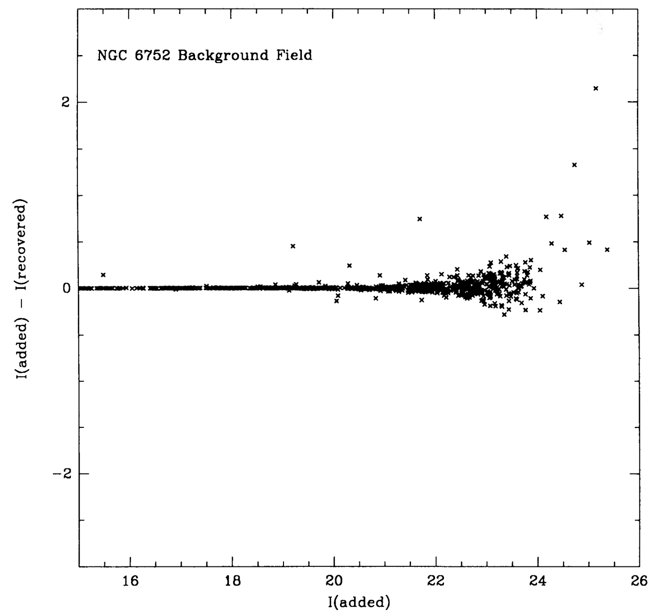

FIG. 3.—Results of the artificial star tests in the background field for NGC 6752.

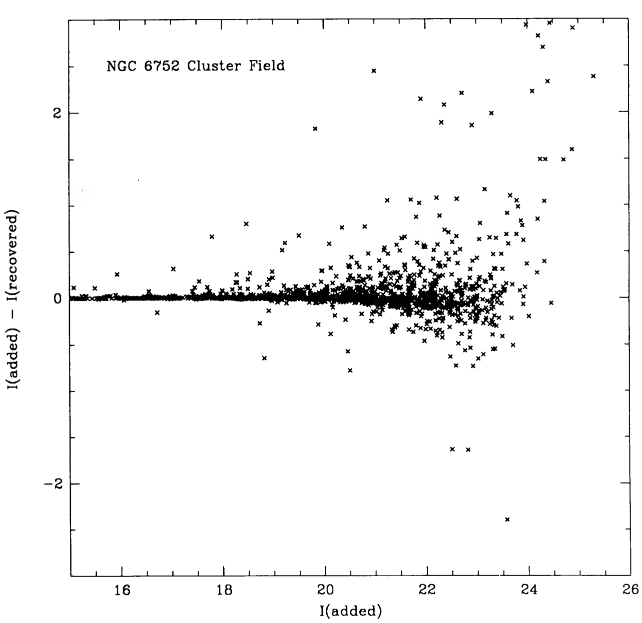

FIG. 2.—Results of the artificial star tests in the cluster field of NGC 6752

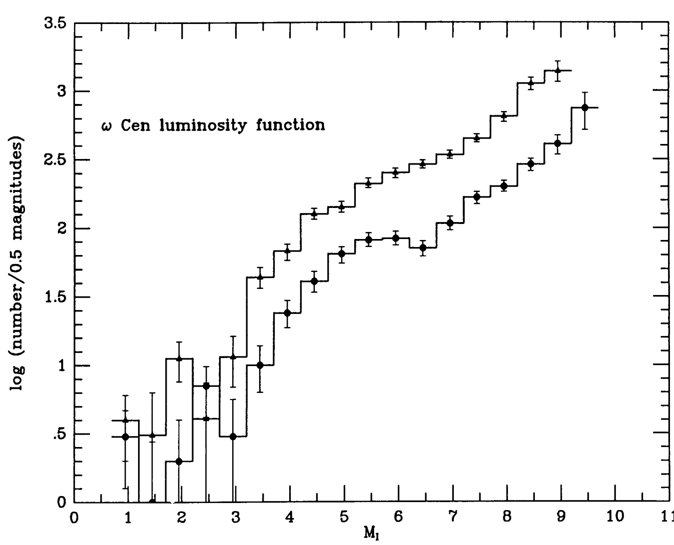

FIG. 4.—Luminosity functions in the I band for two fields in ω Cen. The inner field (*triangles*) is located at 13′.4 (4.96 core radii as defined for the giants; see § 7) from the center (ESO field), while the outer field (*filled circles*) is at 19′ (7.03 core radii for giants) from the cluster core (Las Campanas field).

TABLE 1

ω Centauri Luminosity Function

	Las Campanas Field (4.62 arcmin^2)					ESO Field (5.20 arcmin^2)				
$I(\pm 0.25)$	n_c	In_c	n_b	In_b	Φ	n_c	In_c	n_b	In_b	Φ
14.75	3.0	1.00	0.0	1.00	3 ± 1.7	4.0	1.00	0.0	1.00	4 ± 2
15.25	3.0	1.00	2.0	1.00	1 ± 2.2	7.0	1.00	5.0	1.00	3.1 ± 3.3
15.75	4.0	1.00	0.0	1.00	2 ± 2.0	12.0	1.00	1.0	1.00	11.2 ± 3.6
16.25	8.0	1.00	1.0	1.00	7 ± 3.0	8.0	1.00	5.0	1.00	4.1 ± 3.5
16.75	7.0	1.00	4.0	1.00	3 ± 3.3	17.0	1.00	7.0	1.00	11.5 ± 4.8
17 25	14.0	1.00	4.0	1.00	10 ± 4.2	49.7	1.00	7.0	1.00	44.1 ± 7.4
17.75	28.0	1.00	4.0	1.00	24 ± 5.7	79.0	1.00	15.0	1.00	67.2 ± 9.5
18.25	50.0	1.00	9.0	1.00	41 ± 7.7	139.0	1.00	16.5	1.00	126.0 ± 12.3
18.75	79.0	1.00	15.0	1.00	64 ± 9.7	157.3	1.00	19.3	1.00	142.1 ± 13.1
19.25	87.0	1.00	8.0	1.00	81 ± 9.9	226.6	1.02	19.5	1.00	211.2 ± 15.8
19.75	103.0	1.00	19.0	1.00	84 ± 11.1	269.4	1.05	26.5	1.00	248.4 ± 18.2
20.25	89.0	1.00	18.0	1.00	71 ± 10.3	311.3	1.06	25.0	1.00	291.5 ± 19.8
20.75	153.0	1.00	46.0	1.00	107 ± 14.1	370.6	1.11	43.0	1.01	336.7 ± 23.7
21.25	206.3	1.04	40.3	1.00	166.0 ± 16.0	485.7	1.18	51.0	1.03	445.4 ± 31.3
21.75	252.7	1.04	52.4	1.00	200.3 ± 19.3	706.6	1.38	76.6	1.03	646.1 ± 51.3
22.25	365.2	1.37	77.1	1.04	288.1 ± 27.8	1184.8	2.18	84.6	1.05	1117.9 ± 126.4
22.75	474.4	2.51	69.7	1.42	404.7 ± 60.0	1483.9	4.03	123.3	1.56	1386.5 ± 244.0
23.25	877.2	5.37	144.0	2.57	733.2 ± 211.3	1119.0	5.45	338.5	4.35	851.6 ± 247.9

unity as they were derived from an average of all the ADDSTAR frames after subtraction of the added stars. This procedure was followed to ensure that the ADDSTAR statistics were calculated in a way consistent with the counts for the real stars. At the faint end some of the incompleteness corrections are quite large (both for this cluster and in particular for the background field in M5). These corrections, however, generally have statistical uncertainties associated with them of less than about 25%. For the ω Cen ESO data, because the frames were shifted after each exposure, the final cluster field covered only 79% of the area of that in the background frame. To convert the apparent magnitudes into absolute magnitudes, a distance modulus in I for ω Cen of 13.8 was assumed. This comes from assigning the horizontal branch an M_V of $+0.6$, adopting a reddening $E(B-V)$ of 0.11, and using $A_I = 0.6A_V$ (Richer et al. 1990; Webbink 1985).

The morphology of both luminosity functions is similar with no evidence of a flattening in the star counts down to the faintest objects. The inner curve has some suggestion of a plateau between M_I 5 and 7 followed by a fairly steep rise to the limit of the data.

4.2. *Luminosity Function for M5*

Table 2 contains the star counts and luminosity function for M5, the columns being the same as those in Table 1. The one exception is that in this case the bins are 0.25 mag wide for all entries fainter than 17.25, the brighter bins being 0.5 mag wide. Figure 5 displays the derived luminosity function under the assumption that the cluster distance modulus in I is 14.3. It is similar to that for ω Cen in that there is no evidence of a flattening of the luminosity function at the faint end even though the overall slope is not as steep.

4.3. *Luminosity Function for NGC 6752*

Because of its proximity to us as well as due to the quality of the data that we were able to obtain, the luminosity function for NGC 6752 descends the deepest down the main sequence of the three clusters discussed here. The details of the derivation are included in Table 3, while the function is displayed in Figure 6. The derived apparent distance modulus in I was 13.3. This luminosity function reaches $M_I = 10.25$, and, as can be seen, there is again no evidence of a flattening of this function at the faintest magnitudes. It can be anticipated that the resulting mass function will be quite steep as theoretical luminosity functions, even for quite steep mass function slopes, flatten significantly below an absolute I magnitude of about 8.5 which corresponding to an absolute V magnitude of about 10 (Drukier et al. 1988).

TABLE 2

M5 Luminosity Function (6.55 arcmin^2)

$I(\pm 0.125)$	n_c	In_c	n_b	In_b	Φ
15.0 ± 0.25	1.8	1.00	1.0	1.00	0.8 ± 1.7
15.5 ± 0.25	4.0	1.00	0.0	1.00	4.0 ± 2.0
16.0 ± 0.25	4.0	1.00	1.0	1.00	3.0 ± 2.2
16.5 ± 0.25	3.0	1.00	2.0	1.00	1.0 ± 2.2
17.0 ± 0.25	6.1	1.00	2.0	1.00	4.1 ± 2.8
17.375	10.0	1.00	1.0	1.00	9.0 ± 3.3
17.625	7.0	1.00	1.0	1.00	6.0 ± 2.8
17.875	22.8	1.00	2.0	1.00	20.8 ± 5.0
18.125	19.0	1.00	1.0	1.00	18.0 ± 4.5
18.375	27.3	1.00	1.3	1.00	26.0 ± 5.3
18.625	48.0	1.00	4.5	1.00	43.5 ± 7.3
18.875	43.5	1.00	3.5	1.00	40.0 ± 6.9
19.125	42.5	1.00	3.5	1.00	39.0 ± 6.8
19.375	52.8	1.00	2.3	1.00	50.5 ± 7.4
19.625	61.4	1.00	5.0	1.05	56.4 ± 9.6
19.875	71.8	1.00	9.0	1.00	62.8 ± 9.0
20.125	84.2	1.00	3.0	1.00	81.2 ± 10.7
20.375	81.5	1.00	7.3	1.00	74.3 ± 9.4
20.625	80.8	1.00	11.8	1.00	69.0 ± 9.6
20.875	94.5	1.02	6.1	1.05	88.5 ± 12.6
21.125	84.3	1.03	5.1	1.03	79.1 ± 10.3
21.375	111.4	1.06	6.8	1.05	104.5 ± 12.0
21.625	119.9	1.02	11.9	1.08	108.1 ± 11.8
21.875	151.9	1.15	9.7	1.30	142.2 ± 15.9
22.125	182.4	1.31	13.4	1.92	168.9 ± 21.3
22.375	185.6	1.37	25.0	2.63	160.7 ± 22.8
22.625	249.1	1.47	44.1	3.87	204.9 ± 33.2
22.875	295.6	1.83	69.1	5.04	226.5 ± 52.0
23.125	344.8	2.52	126.5	7.14	218.3 ± 70.9

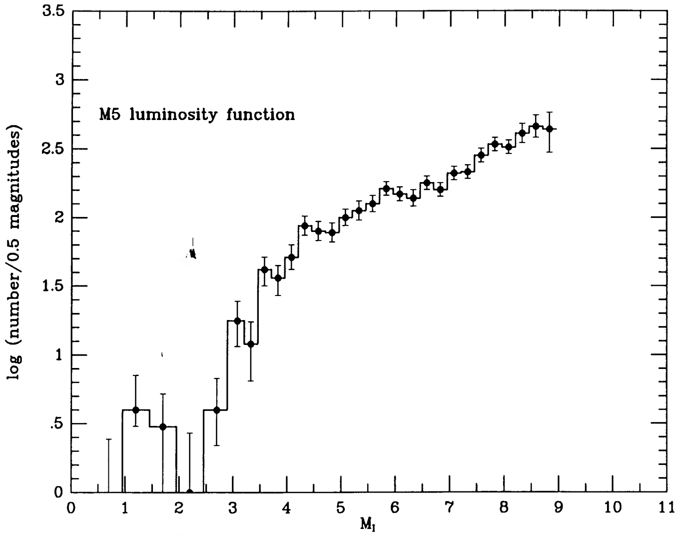

FIG. 5.—The luminosity function in the I band for a single field at 400″ west of the center (about 14 core radii) in M5.

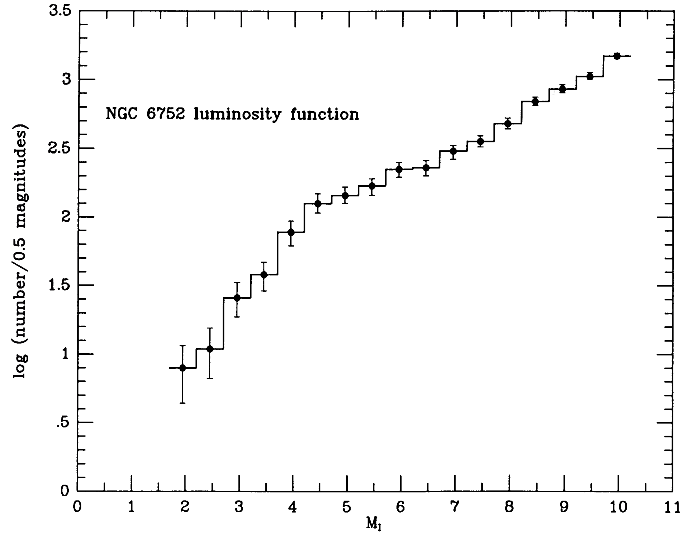

FIG. 6.—The luminosity function in the I band for a single field at about 4′ east of the center (8 core radii assuming a core radius of 30″) in NGC 6752.

5. THE CLUSTER MASS FUNCTIONS

To convert the cluster luminosity functions into mass functions, mass-luminosity relations appropriate to the cluster metal abundances are required. The three clusters discussed here all have rather similar abundances (within about 0.2–0.3 dex), so the same mass-luminosity relation was used. This relation is the one discussed in Fahlman et al. (1989) and presented in tabular form by Brewer (1991) and is appropriate for stars with $[M/H] = -1.5$.

5.1. *Mass Function for ω Centauri*

The derived mass functions for the two fields in ω Cen are displayed in Figure 7. The data for the inner field are plotted with closed triangles while the outer mass function is indicated with filled circles. Note that the last point for the inner field lies on the error bar for the last point in the outer field. The indicated error bars include errors only for the luminosity function; the mass-luminosity relation was assumed to be error-free. One obviously important point about this figure is the excellent agreement between the two mass functions which were derived with different telescopes and CCD chips. From about 0.7 $M_\odot$ down to 0.4 $M_\odot$, both functions are rather flat. Below a mass of about 0.4 $M_\odot$, the mass function in both fields steepens dramatically. This is similar in behavior to what we observed in the three clusters discussed in Richer et al. (1990). As we have mentioned already several times (Richer et al. 1990; Richer & Fahlman 1991), *the upturn in these mass functions occurs disturbingly close to a change in slope in the mass-luminosity relations, so that the possibility cannot be dismissed that the rapid increase to low masses may reflect some inadequacy in the current stellar models.* Although we will continue to interpret this upturn as a real effect, the cautionary note sounded above should be kept in mind.

The apparent power-law slope that we see at the low mass end in both ω Cen mass functions covers the mass range from 0.42 to 0.18 $M_\odot$. To derive the slope over this mass range, we combined the two mass functions together by normalizing them to the same number of stars. As can be judged from

TABLE 3

NGC 6752 LUMINOSITY FUNCTION (6.55 arcmin^2)

$I(\pm 0.25)$	n_c	In$_c$	n_b	In$_b$	Φ
15.25..........	9.0	1.00	1.0	1.00	8.0 ± 3.3
15.75..........	12.0	1.00	1.0	1.00	11.0 ± 3.6
16.25..........	29.0	1.00	3.0	1.00	26.0 ± 5.7
16.75..........	40.0	1.00	2.0	1.07	38.0 ± 6.5
17.25..........	79.0	1.00	1.0	1.00	78.0 ± 8.9
17.75..........	130.3	1.02	3.1	1.04	127.2 ± 20.5
18.25..........	147.0	1.05	1.0	1.00	146.0 ± 21.3
18.75..........	174.9	1.04	6.0	1.00	168.8 ± 23.3
19.25..........	227.7	1.01	6.0	1.00	221.6 ± 28.5
19.75..........	237.6	1.03	10.3	1.03	227.4 ± 28.5
20.25..........	311.1	1.08	12.4	1.03	298.8 ± 34.6
20.75..........	362.3	1.13	7.4	1.05	354.9 ± 33.6
21.25..........	498.3	1.14	20.4	1.02	477.9 ± 43.6
21.75..........	726.3	1.28	28.8	1.03	697.7 ± 50.0
22.25..........	885.9	1.52	32.0	1.03	853.9 ± 51.5
22.75..........	1096.4	1.85	38.4	1.17	1058.1 ± 57.0
23.25..........	1543.3	3.05	73.2	1.44	1470.1 ± 72.7

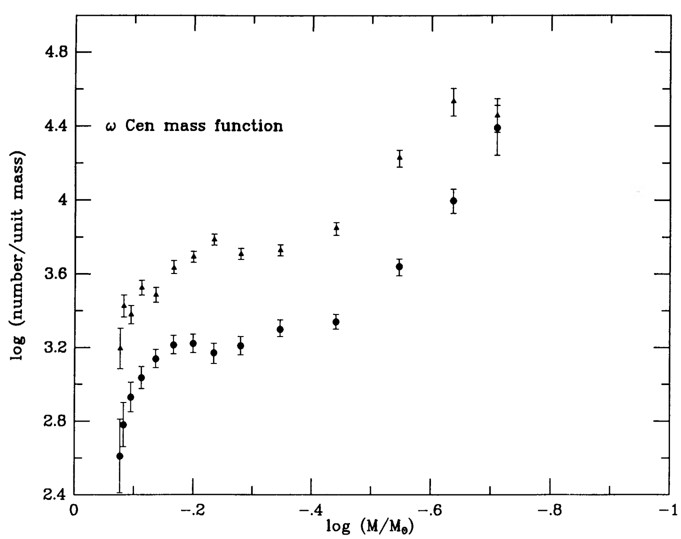

FIG. 7.—Mass functions for the two fields in ω Cen with the triangles for the inner field and the filled circles for the outer one.

Figure 1 (and as can be confirmed in Fig. 7), the expected amount of mass segregation between the two fields for these low-mass stars is small, so very little will be lost in combining the two mass functions. If we define the mass function slope in the normal manner, that is $dN = AM^{-x} d \log(M)$, then the mass function slope for ω Cen over the mass range indicated above is $x = 2.1$. By comparison, the Salpeter slope for the mass function in the solar neighborhood is $x = 1.35$. The mass function slope found here for ω Cen is somewhat flatter than the value we reported in Richer & Fahlman (1991), but the current result should be more reliable being based on two fields and much more extensive incompleteness corrections. We discuss the possible significance and implication of this steep slope in the following section after reviewing the mass function for M5 and NGC 6752.

5.2. *Mass Function for M5*

Figure 8 contains a plot of the mass function derived for the field observed with the NTT in M5. This function is plotted with closed circles. It is morphologically similar to that for ω Cen being rather flat at the high-mass end, and then rising steeply below 0.4 $M_{\odot}$ to the limit of the data. The lowest mass stars observed here are only 0.23 $M_{\odot}$, so the upturn does not quite cover a factor of 2 in mass. The result of this is that the derived mass function slope from these data alone below 0.4 $M_{\odot}$ must be considered quite uncertain. Using the four lowest mass points, we formally obtain that x is 1.3 for the stars in this field of M5, right at the Salpeter value. Also shown for comparison (*closed triangles*) is the function derived from the V data of Richer & Fahlman (1987). These latter points (arbitrary scaling) are from the middle field discussed in that paper and come from stars at about 21 core radii from the center of the cluster. Mass segregation among the most massive objects produces the discrepancy seen at the high-mass end, while the mass function slopes from the two fields at low mass are very similar. This is entirely in accord with expectations (see Fig. 1 for comparison). An important aspect of this comparison is that one mass function is derived from data in the I bandpass with a mass-luminosity relation combining theory and observations (Fahlman et al. 1989; Brewer 1991), while the other mass function comes from V data with a purely theoretical mass function (see Drukier et al. 1988). That they agree so well at the low-mass end is evidence that these mass-luminosity relations are consistent with each other.

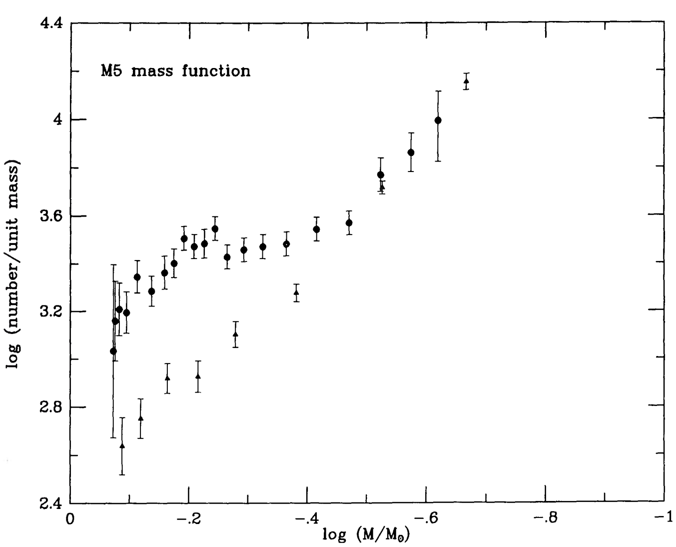

FIG. 8.—Mass functions for M5. The closed circles represent I data from the NTT (14 core radii) while the filled triangles come from V data at 21 core radii (Richer & Fahlman 1987). An arbitrary scaling was applied to the mass function derived from the V data. The effects of mass segregation can be clearly seen among the high-mass stars. Note the striking similarly between this figure and Fig. 1.

5.3. *Mass Function for NGC 6752*

The derived mass function for the field in NGC 6752, shown in Figure 9, covers the largest range in mass of all the three clusters discussed here, ranging from 0.83 $M_{\odot}$ at the high-mass end, down to 0.17 $M_{\odot}$. The steep rise seen below 0.4 $M_{\odot}$ thus covers almost a factor of 2.5 in mass, and hence the derived slope here should be quite reliable. From the most massive stars seen down to 0.4 $M_{\odot}$, the mass function slope is very flat with the formal value of x being about 0.2. This slope is similar to, although a bit flatter than that found by Piotto & Ortolani (1990) over approximately the same mass range. Their data, however, just failed going deep enough to see the steep upturn in the mass function. The slope of the NGC 6752 mass function below 0.4 $M_{\odot}$ to the limit of our data at 0.17 $M_{\odot}$ is a very steep 2.5.

All the data on the cluster mass functions are presented in Tables 4A–4C, wherein N is the number of stars per solar mass. In the following section we compile data on the clusters studied here as well as on the three discussed in Richer et al. (1990) and make an attempt to interpret the steep slopes found in terms of the clusters' IMFs and implications these results might have on the halo mass function and the Galactic dark matter.

6. THE ENSEMBLE OF GLOBULAR CLUSTER MASS FUNCTIONS

At present there are only six globular clusters whose mass functions have been measured to well below 0.4 $M_{\odot}$. In every case the mass function morphology is similar, a rather flat portion from the most massive stars still on the main sequence down to about 0.4 $M_{\odot}$, and a very steep rise below this mass to the limit of the data. A mosaic of all these six mass functions is illustrated in Figure 10. *In no case is there any evidence of a flattening of the mass function at the low-mass end, even though several cluster mass functions extend to within several hun-*

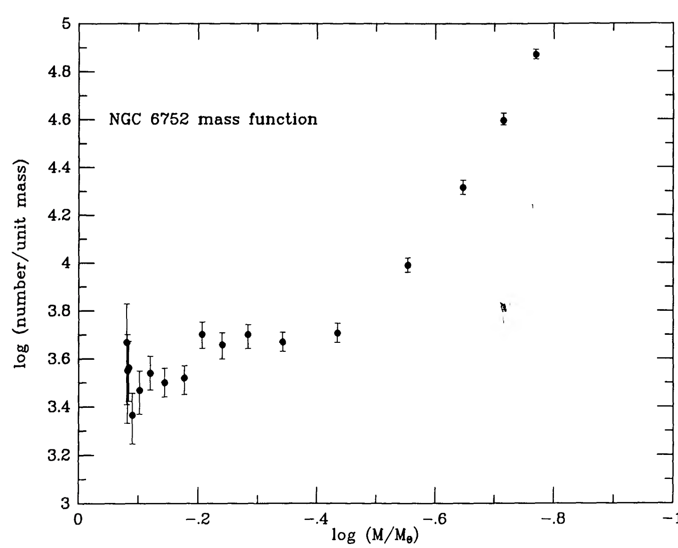

FIG. 9.—Mass function for the field in NGC 6752

TABLE 4A

ω CENTAURI MASS FUNCTION

log m ($M_\odot$)	Las Campanas (log N)	ESO NTT (log N)
−0.077	2.610	3.193
−0.083	2.780	3.424
−0.095	2.929	3.377
−0.113	3.035	3.523
−0.137	3.138	3.484
−0.167	3.214	3.630
−0.200	3.221	3.692
−0.235	3.171	3.785
−0.280	3.209	3.707
−0.347	3.299	3.728
−0.441	3.340	3.849
−0.547	3.641	4.229
−0.637	3.998	4.533
−0.710	4.391	4.456

TABLE 4B

M5 MASS FUNCTION

log m ($M_\odot$)	log N
−0.073	3.033
−0.076	3.158
−0.083	3.207
−0.095	3.193
−0.113	3.344
−0.137	3.283
−0.159	3.361
−0.175	3.401
−0.192	3.505
−0.209	3.471
−0.226	3.483
−0.244	3.546
−0.265	3.427
−0.293	3.457
−0.325	3.471
−0.365	3.482
−0.416	3.544
−0.471	3.570
−0.524	3.770
−0.575	3.862
−0.620	3.994

TABLE 4C

NGC 6752 MASS FUNCTION

log m ($M_\odot$)	log N
−0.08	3.67
−0.08	3.55
−0.08	3.56
−0.09	3.37
−0.10	3.47
−0.12	3.54
−0.14	3.50
−0.18	3.52
−0.21	3.70
−0.24	3.66
−0.28	3.70
−0.34	3.67
−0.44	3.71
−0.55	3.99
−0.65	4.32
−0.72	4.60
−0.77	4.87

dredths of a solar mass of that of brown dwarfs. The cluster mass functions have the general appearance of a sum of two Gaussians (or power laws), with the peak of the high-mass Gaussian occurring near 0.6 $M_\odot$, the two Gaussians overlapping near 0.4 $M_\odot$, and a low-mass Gaussian peaking somewhere below 0.12 $M_\odot$, likely in the brown dwarf regime. This general picture is not dissimilar to that found in the solar neighborhood (Kroupa, Tout, & Gilmore 1990). This suggests that globular cluster masses may be dominated by brown dwarfs from the low-mass Gaussian. A self-consistent model of M13 seems to agree with this picture (Richer & Fahlman 1991). A similar analysis for ω Cen carried out in § 7 below will confirm this scenario. With this in mind, we will only consider in the following investigation the cluster mass function slopes below 0.4 $M_\odot$, as it is the mass below this limit which is likely to dominate the mass of the cluster, or at least dominated it when the cluster was first formed.

Although the total sample size is rather modest, it seems timely to investigate the properties of these clusters to see if any patterns are emerging. Any existing correlations may give a hint to star formation processes in globular clusters or dynamical evolution of these systems. We compile the relevant cluster data in Table 5. In this compilation the third column is the logarithm of the cluster half-mass relaxation time (years) from Binney & Tremaine (1987), while the fifth, sixth, and seventh columns are the cluster concentration parameter and metal abundance from Webbink (1985), respectively, and the mass-to-visual light ratio calculated from fitting Michie-King models to the cluster data (§ 7 below, and Leonard, Richer, & Fahlman 1991). At least three of the clusters in Table 5 possess power-law deviations from a King model in their inner regions so that the core radius is not well defined for these systems. The entries under c for these clusters depend then on the best-fitting King models. The important entry in the fourth column deserves some explanation.

Recently, AHO modeled the current dynamical state and the rate of destruction of individual globular clusters in the Galaxy. The orbits of the clusters were integrated using initial conditions consistent with the observed cluster properties in a range of Galactic mass models. For each calculated orbit, the rates of destruction of the clusters due to four physical processes was calculated. These were (*a*) evaporation from the cluster due to two-body relaxation (a process internal to the cluster), (*b*) dynamical friction which causes a cluster to spiral in toward the Galactic nucleus, and (*c*) and (*d*) two gravitational shocking mechanisms which result from passages through the Galactic disk and from close approaches to the Galactic bulge during perigalacticon. For the clusters of concern in the present work (that is, systems at about the solar distance from the Galactic center), evaporation is the most efficient mechanism of destroying the clusters. For each system AHO calculated a destruction rate which we converted to a

TABLE 5

CLUSTER PROPERTIES

Cluster	x	log $T_{1/2}$	T_D	c	[M/H]	M/L_V
M13	2.7	9.40	7.1	1.4	−1.6	4.1
NGC 6752	2.5	8.94	7.1	1.6	−1.6	...
ω Cen	2.1	0.96	6.7	1.2	−1.6	5.7
M5	1.3	9.44	4.5	1.8	−1.6	...
NGC 6397	0.9	8.47	2.5	1.6	−2.0	...
M71	0.5	8.35	2.9	1.1	−0.5	2.0

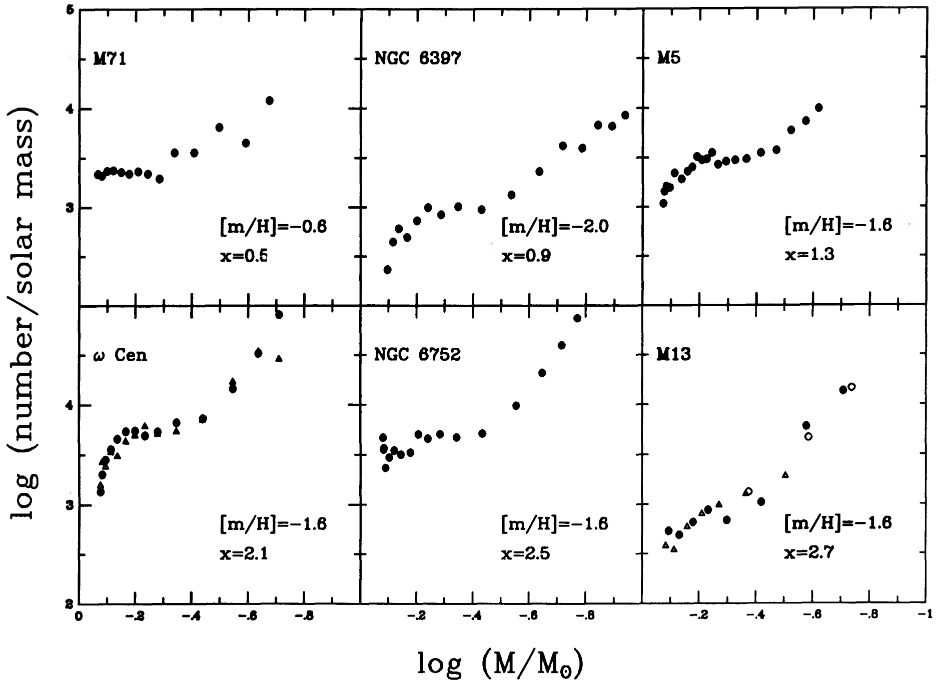

FIG. 10.—Mass function for all six clusters observed in this program thus far. All are based on I band luminosity functions and extend to well below 0.4 $M_\odot$. The two ω Cen and three M13 mass functions were each normalized to represent the same number of stars in each respective field. The cluster metal abundance is indicated as well as the mass function slope x below 0.4 $M_\odot$.

"time until destruction" (simply the inverse of their total destruction rate) in units of the Hubble time. These numbers are listed as T_D in the fourth column of Table 5.

Examination of Table 5 indicates that there is no correlation between the mass function slope x and either c or the cluster metal abundance. It should be kept in mind that the mass function slope referred to here is likely to be close to the IMF if a single power law is capable of describing globular cluster mass function slopes (at least at the low-mass end), and if the cluster has not been extensively tidally stripped. Even in the presence of tidal stripping, the indicated value of x can be considered a lower limit to the IMF slope as the effect of stripping is to flatten the slope. The entries in Table 5 suggest a weak correlation between x and the half-mass relaxation time, and a strong correlation with T_D. Plots of the relaxation time and T_D against x are shown in Figure 11. If we assume that all globular clusters begin life with similar mass function slopes (somewhere near 3), then we can understand (qualitatively) the correlations seen in Figure 11. Due to dynamical processes, the IMF slopes are modified, the left-hand panel suggesting that internal relaxation is important in modifying these slopes, but that more processes are at play. The right-hand panel indicates the very strong correlation between the currently observed mass function slopes and all the processes thought to be important in modifying cluster mass functions.

If this picture is basically correct, there may be important implications for the stellar content of the Galactic halo. If the halo and the clusters have similar mass functions, then the halo mass function slope is very steep with x near 3. In several clusters the observed mass function extends to within a few hundredths of a solar mass of that of brown dwarfs (Fahlman et al. 1989; Richer et al. 1990), with an extension into the brown dwarf regime suggested by continuity arguments (no physical reason to cut star formation at the hydrogen burning limit). Depending on the lower mass cutoff in this very steep mass function, large values for the halo mass-to-light ratio can then be derived with obvious implications for the nature of dark matter in the Galactic halo.

7. A SELF-CONSISTENT MODEL FOR ω CENTAURI

An important question to consider at this point is whether the internal dynamics of these clusters is consistent with the derived mass functions, in particular is the observed velocity dispersion compatible with a large fraction of the mass of the

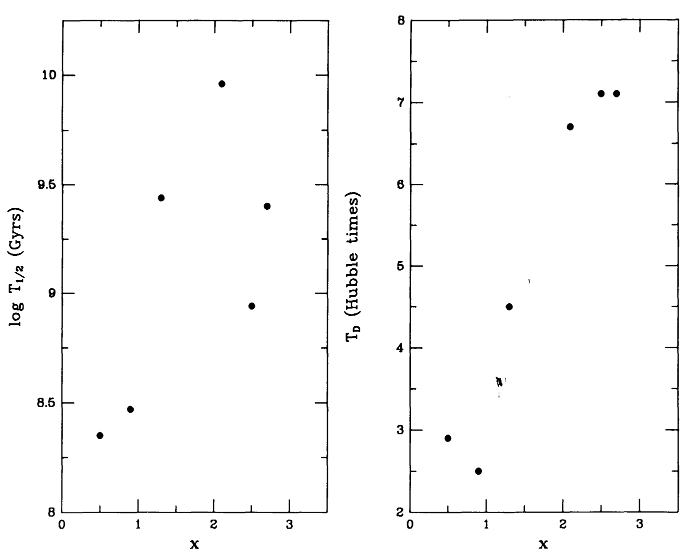

FIG. 11.—Plot of the presently observed mass function slope x below 0.4 $M_\odot$ against the half-mass relaxation time (*left panel*) and the estimated time for the cluster to disrupt (*right panel*).

cluster in very low mass stars. We have already addressed this somewhat in our discussion of M13 (Richer & Fahlman 1991), but the point is a crucial one and here we consider it for ω Cen, a cluster with numerous and accurate radial velocities for individual cluster stars as well as an extensive and accurately determined brightness profile.

Meylan (1987) and Meylan & Mayor (1986) have used CORAVEL radial velocities for stars in ω Cen together with the surface brightness profile to study the cluster's dynamical properties. The cluster mass function was a free parameter in their fits of the data to a King-Michie model. We can improve on this picture by constraining the cluster mass function to agree with what was observed in our two fields, that is a mass function represented by a power-law slope of $x = 2.1$ below 0.4 $M_\odot$, and a slope with $x = -2.35$ for the more massive stars. While this latter value may appear somewhat peculiar, it is required to match what is seen at the high-mass end in our mass function. Clearly a mass function with this slope cannot extend to very high mass. For this reason, an arbitrary scaling was applied to the contribution from each of the two mass functions. The models that we computed were extensions of King (1966) models to include both a mass spectrum and velocity anisotropy (Gunn & Griffin 1979). Seventeen mass classes were used with the lowest mass at 0.05 $M_\odot$, well into the brown dwarf regime. Remnants from massive stars that had completed their main-sequence evolution were also included; these were put into the models with $M = 1.07\ M_\odot$ for stars between 2 and 5 $M_\odot$ and 0.64 $M_\odot$ for stars in the mass range 0.8–2 $M_\odot$. The masses of these remnants were obtained by applying the Iben & Renzini (1983) initial-to-final mass relationship to the stars over these two mass ranges. A scaling between the two mass functions was arranged so that these white dwarfs constituted about 5% of the mass of the model. No heavier remnants were included in the models.

As we discuss these models, we will also consider the methods involved in comparing these multimass models with the data. This point has not been clearly discussed thus far in the literature, and in what follows below we lay out the details. As was shown in Fahlman, Richer, & Nemec (1991), it is often true that a rather wide range of models with very different properties can fit the existing cluster data reasonably well, and simple goodness of fit criteria to choose among them are not particularly illuminating. We generated more than 20 different models in carrying out the analysis for ω Cen, but we will consider only one in detail. It makes the point that is important in the current context; that is, that the known dynamical properties of the cluster are consistent with the presence of a large mass fraction in very low mass stars.

The actual model which we compare with the data below had a central potential $W_0 = 6.0$. The anisotropy radius was set at 2.5 scale radii (a very anisotropic model, consistent with the suggestion of Meylan 1987), and 17 mass classes were used with the low-mass cutoff set at 0.05 $M_\odot$ resulting in just over 40% of the cluster mass being contained in brown dwarfs. Models with the central potential in the range 8–5.5, anisotropy radii from infinity (no anisotropy), through 2 scale radii, and various weightings between the two power laws making up the mass function were calculated. Some fit reasonably well, others were poor, and from simple eyeball estimates, the one illustrated here seemed to be the best, but no great statistical significance should be given to this.

The first step in comparing a King model with the observed data is to establish a scaling between the dimensionless radii returned by the model, and the physical scale of the data. This is accomplished by fitting the model radial density profile to the observed brightness distribution. The vertical scale factor is arbitrary because the data are essentially uncalibrated, but the horizontal scale factor can be found. The fit for the model considered is shown in Figure 12 with the data from Meylan (Table 1). In this comparison a scale radius of 3′.475 per dimensionless unit of the model was applied. At the assumed distance of the cluster (5200 pc; Webbink 1985), this corresponds to 5.256 pc. This quantity does not correspond to anything physical; in particular, it is *not* the core radius of the cluster. The effective core radius is defined as the radius at which the projected number density falls to half its central value. This radius is, of course, different for each of the 17 mass species. In the model under consideration, the core radius is 4.09 pc for the giants and their concentration parameter ($c = \log r_t/r_c$) is 1.33.

Comparison of the data with a King model proceeds by determining the value of the central surface density of the cluster in physical units ($M_\odot$ pc^{-2}). This effectively ties the data to the model. The derivation of the central surface density is accomplished by determining the ratio $f_r = \sigma_k(r)/\sigma_k(0)$, where $\sigma_k(r)$ is the surface mass density contributed by mass class k at a radius r from the cluster and $\sigma_k(0)$ is the same quantity at the cluster center. The ratio f_r is strictly a model parameter; however, once obtaining it, by then using a value of $\sigma_k(r)$ derived from the data, the central surface mass density can be arrived at. Specifically, the model discussed above had a central surface density for mass class 12 (0.29 $M_\odot$) of -1.504 in the log (arbitrary units) while the value at 3.856 scale radii (equal to 20.267 pc or 13′.400) was -2.713. This distance corresponds to the location of the ESO field from the cluster center. Thus f_r for this mass class and distance is 0.06177. From the data we can also determine an observational value of $\sigma_k(r)$. The number of 0.29 $M_\odot$ stars found in the field was 1117.9 (this

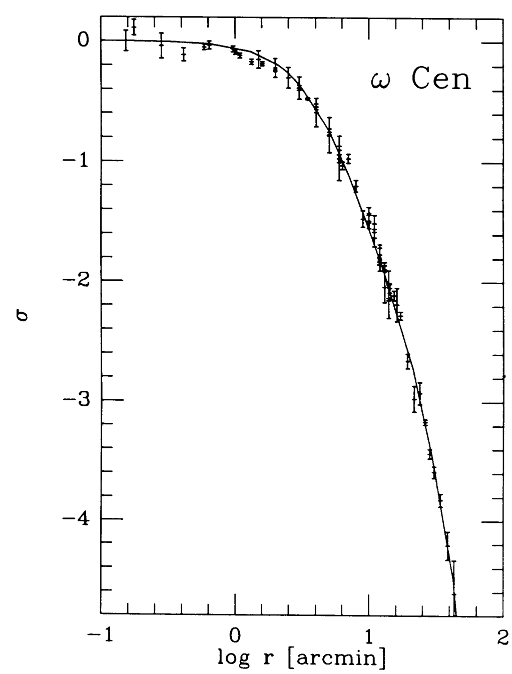

FIG. 12.—Brightness profile for ω Cen. The data are from Meylan (1987), and the solid line is the projected density (for giants) from the multimass King model discussed in the text.

mass corresponds to stars with I in the range 22.00–22.50; see Table 1). With a field area of 5.201 arcmin^2, corresponding to 11.905 pc^2, this results in an observed surface mass density of 17.23 $M_\odot$ pc^{-2}. Using the value of f_r found above, we derive a central surface mass density for this mass class of 440.83 $M_\odot$ pc^{-2}. To derive the total central surface mass density σ_0 we can write that mass class k contributes some fraction f_0 of the total projected density at the center, namely $f_0 = \sigma_k(0)/\sigma_0 = m_k \times n_{0,k}/p$, where $n_{0,k}$ is the projected number density at the center and p is the projected density of the model. The parameter p is returned by the model and for the one under consideration it is 1.844. The value of $\sigma_k(0)$ comes from the projected mass density for each mass class, also returned by the model. For mass class 12, f_0 has the value 0.01698 so that the total central surface mass density is 25,962.6 $M_\odot$ pc^{-2}. In practice the above procedure can be repeated for as many mass classes as possible and the results averaged.

The central density of the cluster then follows directly from the expression $\rho_0 = \sigma_0/p \cdot r_s$, where r_s is the scale radius in pc. For the numbers used above, this results in a central mass density of 2,678.7 $M_\odot$ pc^{-3}. The scaling factor for the velocity dispersion can then be obtained from $V_s^2 = 6 \times 10^{-3} \rho_0 r_s^2$ (King 1966, eq. [15]), which yields $V_s = 21.07$, this number multiplying the dimensionless velocity dispersion returned by the model. This provides a crucial test of the model, a comparison of the model velocity dispersion as a function of radius with that observed from radial velocities of individual stars. This comparison is illustrated in Figure 13 where the model velocity dispersion scale as described above is overlaid (there are now no free parameters) on the observational velocity dispersion taken from Meylan & Mayor (1986, Table 4A). The actual scaling factor used in this comparison is an average over all the mass classes below 0.4 $M_\odot$ for the two fields observed.

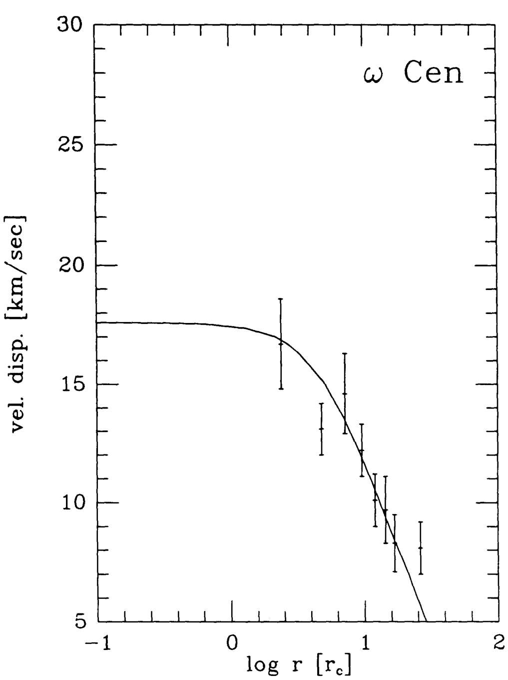

FIG. 13.—Velocity dispersion profile (*solid line*) as a function of the logarithm of the core radius (for giants). The data are from Meylan & Mayor (1987, Table 4A). There are no free parameters in this comparison. The excellent agreement between the two implies that the cluster dynamics are consistent with roughly half the cluster mass contained in brown dwarfs.

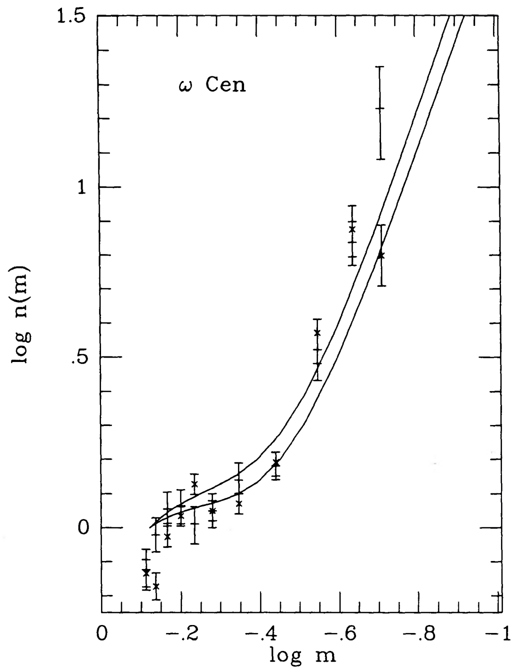

FIG. 14.—Observed mass functions in the two fields of ω Cen compared with theoretical mass functions at radii which bracket the positions of these fields.

This is the crucial test. *This diagram illustrates that a mass function for ω Cen that is dominated by very low mass stars is consistent with the cluster dynamics.*

A last comparison of the model with the data is shown in Figure 14 where the observed mass function in the two fields (scaled so that they have the same number of stars) is compared with that predicted from the model in these fields (the vertical scaling between the data and theory here is arbitrary). The agreement between the two mass functions is quite good over the entire mass range. At the low-mass end, the data seem to require a model that is slightly steeper than was input. This would make the low-mass stellar contribution to the global cluster mass even larger, perhaps increasing the cluster mass-to-light ratio derived below.

We can now use this model (which clearly represents the data rather well), to derive a mass-to-light ratio for ω Cen. The cluster mass is given by $M_c = \mu r_s^3 \rho_0$, where μ is a model parameter (King 1966) and has the value 18.343 for the model discussed here. This yields a total mass for ω Cen of 7.13×10^6 $M_\odot$, a somewhat higher value than normally found in the literature, about a factor of 2 higher than most models derived by Meylan & Mayor (1986). With a luminosity in the V band in solar units of 1.25×10^6 $L_\odot$ (Webbink 1985), a remarkably high mass-to-light ratio of 5.71 is obtained. While larger than most estimates for Population II samples, it is similar to what we obtained for M13 (Richer & Fahlman 1991).

8. DISCUSSION

From mass functions in six globular clusters extending in all cases to well below 0.4 $M_\odot$, we have searched for any correlations between the slopes of these functions and cluster parameters. The aim here is to provide some input into questions relating to star formation scenarios in the early universe, the origin of cluster mass function slopes, and the origin and stellar content of the Galactic halo. As a first step in the process, we emphasized again that mass function slopes derived at large core radii for low-mass stars in globular clusters should be quite close to the cluster IMFs in the absence of tidal stripping. This is an important result allowing an estimation of the cluster IMF slope without knowledge of the complete dynamical history of the object. What has come out of this study and two earlier ones is that all six deep globular cluster mass functions seem to turn up sharply below 0.4 $M_\odot$, and that none of the functions flatten before the limit of the data are reached. While quite speculative, the appearance of the mass functions is not inconsistent with the sum of two Gaussians which cross at about 0.4 $M_\odot$.

The mass functions at the low-mass end seem to display a range of slopes which are uncorrelated with either cluster metal abundance or concentration parameter. A weak correlation is seen with the half-mass relaxation time, and a strong one with the estimated time for the cluster to disrupt. While the details are still lacking, a scenario in which clusters form with similar mass functions which are then modified by dynamical evolution of the cluster, may best represent the emerging data. An extension of the AHO work to include a realistic mass spectrum for each cluster would be very valuable, allowing the evolution of the mass function slope to be followed. Some progress toward this was initiated by Lee, Fahlman, & Richer (1991) who produced a series of models describing the dynamical evolution of globular clusters with a mass spectrum. The orbital characteristics of the clusters was simpler than that in AHO, in that a steady Galactic tidal field was imposed. While no models with very steep IMFs were considered in the work of Lee et al. (1991), the evolution of the mass function of a cluster with an original slope of $x = 1$ was followed. In this cluster, which ended up in a post–core collapse phase and which had lost 84% of its mass after one Hubble time, the mass function slope at the low-mass end (at about the cluster half-mass radius) had decreased from 1 to about 0. The properties of this cluster are very roughly similar to M71 which is also thought to have lost a major fraction of its original mass (Lee et al. 1991). While a quantitative comparison here would be premature, it is of interest to note that a cluster evolving dynamically can change its mass function slope significantly in the direction suggested by the current observations.

Of particular interest regarding these observations is the possible relation between globular cluster mass functions and the halo mass function. If these are similar, then there are important implications for the nature of the dark matter in the Galactic halo. In particular, if the model for ω Cen derived in § 7 also applies to the Galactic halo, then a leading candidate for the halo dark matter is low-metallicity brown dwarfs, a picture consistent with evidence from quasar microlensing (Rix & Hogan 1988). While the derived mass-to-light ratio for ω Cen is less than 6 whereas the halo value may be in the range of 50–100, it should be kept in mind that the currently observed low mass content of these clusters may not be their initial ones. Large numbers of their lowest mass stars may have been lost in the subsequent dynamical evolution of these systems, thus decreasing their mass-to-light ratios. With a halo mass function slope of $x = 2.5$ and a local density of halo dwarfs with masses greater than 0.25 $M_\odot$ of 0.8×10^{-4} $M_\odot$ pc^{-3} (Schmidt 1975) it is only necessary to extend the halo mass function down to about 0.02 $M_\odot$ to account for the local dark matter (Lake 1991). Further, as Lake (1991) has repeatedly pointed out, this mass function is not in conflict with the existing searches for low-mass stars. The Boeschaar & Tyson (1983) survey found 4 M stars in a 400 pc^3 volume where only 0.9 were expected with the Schmidt normalization and a mass function slope of 2.5. This may be suggesting that the halo mass function slope is even steeper than this and thus allows the low-mass limit to be larger. While there are several objections to a similar formation scenario for the halo and the globular cluster system (e.g., globular clusters in elliptical galaxies have a more extended spatial distribution than the background stars as well as a flatter density profile [Harris 1986], cluster system about 0.5 dex more metal-poor on average than the halo [Hanes & Brodie 1986; Huchra & Brodie 1987; Mould, Oke, & Nemec 1987; Brodie & Huchra 1991]), many of these can be explained in terms of a difference between the dynamical evolution of the cluster system compared to the lack of such evolution for individual stars comprising the halo. Until a clear picture emerges for the formation of the halo and the system of globular clusters, or until their mass functions are actually measured to be different, the simplest assumption is to assume that the mass functions for both of these are similar.

The authors are indebted to ESO and Las Campanas for making telescope time available for their globular cluster program. Thanks are also due to Patrick Cote who carried out some of the reductions discussed herein. The research of G. G. F. and H. B. R. is supported by grants from the Natural Sciences and Engineering Research Council of Canada.

REFERENCES

Aguilar, L., Hut, P., & Ostriker, J. 1988, ApJ, 335, 720 (AHO)
Alcaino, G., & Liller, W. 1984, AJ, 89, 1712
———. 1987, AJ, 94, 1585
Bahcall, J. N., & Soneira, R. M. 1981, ApJS, 47, 357
Binney, J., & Tremaine, S. 1987, Galactic Dynamics (Princeton: Princeton Univ. Press), 514
Boeshaar, P. C., & Tyson, J. A. 1983, in The Nearby Stars and the Stellar Luminosity Function, ed. A. G. D. Philip & A. R. Upgren (Schenectady: L. Davis), 85
Boeshaar, P. C., Tyson, J. A., & Seitzer, P. 1986, in Astrophysics of Brown Dwarfs, ed. M. C. Kafatos, R. S. Harrington, & S. P. Maran (London: Cambridge Univ. Press), 76
Brewer, J. 1991, M.Sc. thesis, University of British Columbia
Brodie, J. P., & Huchra, J. P. 1991, preprint
Buonanno, R. 1988, in ESO Midas Manual (Graching: ESO), chap. 5
Campbell, B., Walker, G. A. H., & Yang, S. 1988, ApJ, 331, 902
Cannon, R. D., & Stobie, R. S. 1973, MNRAS, 162, 227
Chiu, L. G. 1980, AJ, 85, 812
Cowie, L. L., Lilly, S. J., Gardner, J. P., & McLean, I. S. 1988, ApJ, 332, L29
D'Antona, F. 1987, ApJ, 320, 653
Dawson, P. C. 1986, ApJ, 311, 984
Djorgovski, S., & King, I. R. 1986, ApJ, 305, L61
Drukier, G. A., Fahlman, G. G., Richer, H. B., & VandenBerg, D. A. 1988, AJ, 95, 1415
Fahlman, G. G., Richer, H. B., & Nemec, J. 1991, ApJ, 380, 124
Fahlman, G. G., Richer, H. B., Searle, L., & Thompson, I. B. 1989, ApJ, 343, L49
Fich, M., & Tremaine, S. 1990, preprint
Gunn, J. E., & Griffin, R. F. 1979, AJ, 84, 752
Hanes, D. A., & Brodie, J. P. 1986, ApJ, 300, 279
Harris, W. E. 1986, AJ, 91, 822
Hartwick, F. D. A., Cowley, A. P., & Mould, J. R. 1984, ApJ, 286, 269
Huchra, J. P., & Brodie, J. P. 1987, AJ, 93, 779
Iben, I., & Renzini, A. 1983, ARAA, 21, 271
Jameson, R. F., Sherrington, M. R., & Giles, A. B. 1983, MNRAS, 205, 39P
King, I. R. 1966, AJ, 71, 64
Kroupa, P., Tout, C. A., & Gilmore, G. 1990, MNRAS, 244, 76
Lake, G. 1991, private communication
Landolt, A. U. 1983, AJ, 88, 439
Larson, R. B. 1976, in Galaxies, ed. L. Martinet & M. Mayor (Geneva: Geneva Observatory), 67
Lee, H. M., Fahlman, G. G., & Richer, H. B. 1991, ApJ, 366, 455

Leonard, P. B., Richer, H. B., & Fahlman, G. G. 1991, in preparation
McClure, R. D., Hesser, J. E., Stetson, P. B., & Stryker, L. L. 1985, PASP, 97, 665
Meylan, G. 1987, A&A, 184, 144
Meylan, G., & Mayor, M. 1986, A&A, 166, 122
Mould, J. R., Oke, J. B., & Nemec, J. M. 1987, AJ, 93, 53
Piotto, G., & Ortolani, S. 1990, preprint
Richer, H. B., & Fahlman, G. G. 1987, ApJ, 316, 189
———. 1991, in The Formation and Evolution of Star Clusters, ed. K. Janes (Boston: ASP), 120
Richer, H. B., Fahlman, G. G., Buonanno, R., & Fusi, Pecci, F. 1990, ApJ, 359, L11
Rix, H. W., & Hogan, C. J. 1988, ApJ, 332, 108
Schild, R. E. 1984, PASP, 95, 1021
Schmidt, M. 1975, ApJ, 202, 22
Searle, L., & Thompson, I. B. 1990, private communication
Searle, L., & Zinn, R. 1978, ApJ, 225, 357
Skrutskie, M. F., Forrest, W. J., & Shure, M. A. 1987, ApJ, 312, L55
Smith, G. H., McClure, R. D., Stetson, P. B., & Hesser, J. E. 1986, AJ, 91, 842
VandenBerg, D. A., & Bell, R. A. 1985, ApJS, 58, 561
Webbink, R. F. 1985, in IAU Symposium 113, Dynamics of Star Clusters, ed. J. Goodman & P. Hut (Dordrecht: Reidel), 541
Wielen, R., Jahreiss, H., & Kruger, R. 1983, in IAU Colloquium 76, The Nearby Stars and the Stellar Luminosity Function (Schenectady: Davis), 163
Zinnecker, H. 1987, in ESO Workshop on Stellar Evolution and Dynamics in the Outer Halo of the Galaxy, ed. M. Azzopardi & F. Matteucci (Garching: ESO), 599